



**HAL**  
open science

## **Atomic distribution and local structure in ice VII from in situ neutron diffraction**

Keishiro Yamashita, Kazuki Komatsu, Stefan Klotz, Oscar Fabelo, Maria T Fernández-Díaz, Jun Abe, Shinichi Machida, Takanori Hattori, Tetsuo Irifune, Toru Shinmei, et al.

► **To cite this version:**

Keishiro Yamashita, Kazuki Komatsu, Stefan Klotz, Oscar Fabelo, Maria T Fernández-Díaz, et al.. Atomic distribution and local structure in ice VII from in situ neutron diffraction. Proceedings of the National Academy of Sciences of the United States of America, 2022, 119 (40), pp.e2208717119. 10.1073/pnas.2208717119 . hal-03879209

**HAL Id: hal-03879209**

**<https://hal.science/hal-03879209>**

Submitted on 30 Nov 2022

**HAL** is a multi-disciplinary open access archive for the deposit and dissemination of scientific research documents, whether they are published or not. The documents may come from teaching and research institutions in France or abroad, or from public or private research centers.

L'archive ouverte pluridisciplinaire **HAL**, est destinée au dépôt et à la diffusion de documents scientifiques de niveau recherche, publiés ou non, émanant des établissements d'enseignement et de recherche français ou étrangers, des laboratoires publics ou privés.

1

2

## 3 **Atomic distribution and local structure in ice VII from in-situ** 4 **neutron diffraction**

5 Keishiro Yamashita<sup>a\*</sup>, Kazuki Komatsu<sup>a</sup>, Stefan Klotz<sup>b</sup>, Oscar Fabelo<sup>c</sup>, Maria T. Fernández-Díaz<sup>c</sup>,  
6 Jun Abe<sup>d</sup>, Shinichi Machida<sup>d</sup>, Takanori Hattori<sup>e</sup>, Tetsuo Irifune<sup>f</sup>, Toru Shinmei<sup>f</sup>, Kazumasa  
7 Sugiyama<sup>g</sup>, Toru Kawamata<sup>g</sup>, and Hiroyuki Kagi<sup>a</sup>

8 <sup>a</sup>Geochemical Research Center, Graduate School of Science, The University of Tokyo, 7-3-1  
9 Hongo, Bunkyo-ku, Tokyo 113-0033, Japan; <sup>b</sup>Institut de Minéralogie, de Physique des Matériaux  
10 et de Cosmochimie (IMPIC), CNRS UMR 7590, Sorbonne Université, Muséum National  
11 d'Histoire Naturelle, 4 place Jussieu, F-75252 Paris, France; <sup>c</sup>Institut Laue-Langevin, 71 avenue  
12 des Martyrs CS 20156, F-38042 Grenoble Cedex 9, France; <sup>d</sup>Neutron Science and Technology  
13 Center, Comprehensive Research Organization for Science and Society (CROSS), IQBRC Bldg,  
14 162-1 Shirakata, Tokai, Naka, Ibaraki 319-1106, Japan; <sup>e</sup>J-PARC Center, Japan Atomic Energy  
15 Agency, 2-4 Shirakata, Tokai-mura, Ibaraki 319-1195, Japan; <sup>f</sup>Geodynamics Research Center  
16 (GRC), Ehime University, 2-5 Bunkyo-cho, Matsuyama, Ehime 790-8577, Japan; <sup>g</sup>Institute for  
17 Materials Research (IMR), 2-1-1 Katahira, Aoba-ku, Tohoku University, Sendai 980-8577, Japan

18 \*Corresponding author

19 **Email:** [Keishiro.Yamashita@uibk.ac.at](mailto:Keishiro.Yamashita@uibk.ac.at)

20 Present address of the corresponding author: Institute of Physical Chemistry, University of  
21 Innsbruck, Innrain 52c, 6020 Innsbruck, Austria

22 **Author Contributions:** K.Y. and K.K. designed and carried out the experiments and their  
23 analyses. K.Y., K.K., S.K., O.F., and M.T.F. performed single-crystal neutron diffraction  
24 measurements. K.Y., K.K., J.A., S.M., and T.H. performed powder neutron diffraction  
25 measurements. T. I., T.S., K.S., and T.K. contribute to the development of the diamond anvil cell.  
26 H.K. directed the research.

27 **Competing Interest Statement:** The authors declare no competing interest.

28 **Classification:** Physical Science / Chemistry

29 **Keywords:** ice, high pressure, neutron diffraction, disordered structure

30 Article published in PNAS, vol. 119 (2022), <https://doi.org/10.1073/pnas.2208717119>

31

32 This article contains supporting information online at

33 <http://www.pnas.org/lookup/suppl/doi:10.1073/pnas.2208717119/-/DCSupplemental>.

## 1 **Abstract**

2 Ice polymorphs show extraordinary structural diversity depending on pressure and temperature.  
3 The behavior of hydrogen-bond disorder is not only a key ingredient for their structural diversity  
4 but also controls their physical properties. However, it has been a challenge to determine the  
5 detail of the disordered structure in ice polymorphs under pressure because of the limited  
6 observable reciprocal space and inaccuracies related to high-pressure techniques. Here we  
7 present the first elucidation of the disordered structure of ice VII, the dominant high-pressure form  
8 of water, at 2.2 GPa and 298 K from both single-crystal and powder neutron diffraction  
9 techniques. We reveal the three-dimensional atomic distributions from the maximum entropy  
10 method and unexpectedly find a ring-like distribution of hydrogen in contrast to the commonly-  
11 accepted discrete sites. In addition, total scattering analysis at 274 K clarified the difference in the  
12 intermolecular structure from ice VIII, the ordered counterpart of ice VII, despite an identical  
13 molecular geometry. Our complementary structure analyses robustly demonstrate the unique  
14 disordered structure of ice VII. Furthermore, these noble findings are related to the proton  
15 dynamics which drastically vary with pressure, and will contribute to an understanding of the  
16 structural origin of anomalous physical properties of ice VII under pressures.

17

## 18 **Significance Statement**

19 Ice VII is a textbook example of a hydrogen-disordered solid, but the exact distribution of  
20 hydrogen atoms is still unknown. Here we report the detailed atomic distribution and local  
21 structure of ice VII revealed from neutron diffraction data of both single-crystalline and powder  
22 specimens under high pressure. Recent technical developments enabled a robust analysis of the  
23 diffraction data: ice VII has a different intermolecular structure from its ordered counterpart, ice  
24 VIII, even at short distances, despite their identical molecular geometry. Moreover, hydrogen has  
25 an unusual ring-like distribution and an elongation toward hydrogen-bonded water molecules. Our  
26 findings highlighted the uniqueness of the disordered structure of dense ice and open the door for  
27 further understanding of network structure in extreme conditions.

28

29

## 30 **Main Text**

31

### 32 **Introduction**

33

34 Water freezes into various solid structures, including crystalline and non-crystalline phases, when  
35 compressed or cooled down. Ice VII is one of its 20 crystalline phases and is stable at room  
36 temperature between 2 and 60 GPa. In this pressure range, ice VII shows various anomalous  
37 behaviors related to pressure-dependent proton dynamics such as a sharpening of the Raman  
38 peak of its symmetric vibration mode at 11–13 GPa(1) which is caused by a cross-over of  
39 dominant processes from molecular rotation to proton translation(2, 3). Ice VII also undergoes a  
40 phase transition involving hydrogen-bond symmetrization toward ice X(4, 5). This anomalous  
41 crystalline phase has attracted much scientific interest, and it hence appears crucial to  
42 understand its detailed structure.

43 The structure of ice VII can be regarded as two interpenetrating diamond-like networks formed by  
44 hydrogen-bonded water molecules (Figure 1a). In each network, water molecules are  
45 orientationally disordered as those in other ice polymorphs (e.g. ordinary ice I<sub>h</sub>(6)). Hydrogens of  
46 each water molecule randomly occupy two of four sites toward the neighboring oxygens. In other  
47 words, the overall structure of ice VII consists of a combination of various configurations. Ice VII  
48 transforms into ice VIII by ordering the hydrogen positions (or molecular orientations) at low  
49 temperatures (below 273 K at 3 GPa(7)). In ice VIII, the orientations of water molecules are well

1 defined: hydrogens occupy two particular sites, and molecular orientations between the  
2 interpenetrating networks are aligned antiparallel along the *c*-axis, which induces displacement of  
3 the network relative to the other along the *c*-axis. This results in a tetragonal distortion of ice VIII.  
4 The disordered structure of ice VII is generally represented by a cubic unit cell with space group  
5  $Pn\bar{3}m$  (#224) in which oxygens locate at 2*a* site, and hydrogens at 8*e* site with occupancy of 0.5  
6 (hereafter, this model is called a “single-site” model). The symmetric constraints simplify the  
7 structure model as it needs only one parameter for the hydrogen position (*x*, *x*, *x*) and two  
8 variables for atomic displacement parameters (ADPs) (three for anisotropic ADPs). The single-  
9 site model reproduces well the diffraction patterns and therefore has been adopted in almost all  
10 previous studies(8, 9). Nevertheless, structure refinements based on the single-site model are  
11 known to cause a highly anomalous geometry of the water molecule, e.g. an unrealistically short  
12 O-D covalent bond length (0.89 Å(10)) compared to those in ice VIII (0.97 Å)(10, 11) whereas a  
13 computational study showed similar distances for both phases(12). This implies that water  
14 molecules in ice VII are not in the positions assumed in the single-site model. The agreement of  
15 the single-site model with the diffraction patterns appears to be a result of time and spatial  
16 averaging in diffraction measurements.

17 On the other hand, more reasonable “multi-site” models have been proposed up to date to  
18 describe the real structure of ice VII. In these models, the hydrogen atoms are located away from  
19 a straight line between adjacent oxygens, especially toward the three non-bonded oxygens  
20 belonging to the other hydrogen-bonding network(13). Oxygen positions were modelled mainly in  
21 two ways: displacements toward  $\langle 111 \rangle$ (14) or  $\langle 100 \rangle$ (10) as illustrated in Figure 1b.

22 Displacements along  $\langle 100 \rangle$  imply that ice VII favours local structures similar to those in the  
23 ordered structure of ice VIII while displacements along  $\langle 111 \rangle$  imply the opposite. The  $\langle 111 \rangle$   
24 model entails differences in hydrogen-bond length: a shorter one in which one oxygen gets close  
25 to the neighbor and a longer one in which oxygen is away from the neighbor (14). The existence  
26 of the bimodal probability of hydrogen-bond length is still controversial (17, 18). However, no  
27 unambiguous structure refinements have been achieved so far because the atomic  
28 displacements from the single-site position are very small (0.1 Å) and this parameter strongly  
29 correlates with ADPs in the structure refinement. A computational study from density functional  
30 theory (DFT) suggested a probability distribution similar to the  $\langle 100 \rangle$  displacement of oxygen  
31 rather than  $\langle 111 \rangle$  although it also insisted that both displacement models are too simplistic(15).  
32 In conclusion, the actual structure in ice VII has not been experimentally proven up to the present.  
33

34 Here we report *in-situ* single-crystal neutron diffraction using a newly developed apparatus.  
35 Previous powder diffraction studies had limitations in resolution related to peak duplicates in one-  
36 dimensional diffractograms, whereas single-crystal diffraction can directly provide discrete  
37 reflection intensities without peak overlap and can lead to a definitive conclusion by double-  
38 checking with the well-established powder diffraction technique(16). In addition to the technical  
39 improvements in measurements, non-conventional analytical approaches are also necessary to  
40 reveal the detailed disordered structure of the dense ice without constraints from structure models  
41 like the single-site model because conventional analyses have considerable difficulties in  
42 modeling the real distribution. We applied a maximum entropy method (MEM) analysis to reveal  
43 three-dimensional atomic distributions in the unit cell. Moreover, information on local structures  
44 like the water geometry was extracted as interatomic correlation by total scattering analysis. For  
45 these approaches, neutron diffraction is suitable for this study owing to its sensitivity to hydrogen  
46 (deuterium). The scattering length does not decay according to  $\sin\theta/\lambda \propto 1/d$  in contrast to x-ray  
47 diffraction. Therefore, numerous reflections are observable even for low *d*-spacing, which allows  
48 a structure analysis with high resolution in real space. Deuterated samples (D<sub>2</sub>O) were used in all  
49 the experiments instead of light water (H<sub>2</sub>O) to avoid incoherent scattering. This isotope  
50 replacement shifts the phase boundary between ices VI and VII toward slightly lower pressure but  
51 does not affect significantly the disordered structures investigated in this study.  
52  
53

## 54 Results

1  
2 The MEM analysis is based on the principle of maximum entropy, a part of Bayesian statistics,  
3 which expects the most probable density distribution to be one with the largest information  
4 entropy under constraints on the observed structure factors  $F_o$  and their uncertainties  $\sigma F_o$ .  
5 Results of MEM analyses on both single crystal and powder diffraction data show ring-like  
6 distributions of deuterium around the  $\langle 111 \rangle$  axes, direction toward the oxygen of hydrogen-  
7 bonded water, away from the position assumed in the single-site model (Figures 2a and 2b), and  
8 the ring is slightly distorted to a triangular shape. Their maxima are displaced from the axes by  
9 0.1–0.2 Å. These are similar to the reported values (13, 14), but such a ring-like distribution can  
10 only be approximately described by the displacement ellipsoid conventionally used in least-  
11 squares structure refinements. The corners of the triangular-like distribution are in staggered  
12 directions to other deuterium sites covalently bonded to the oxygen as previously suspected(13).  
13 From Figures 2c and 2d, the distance between the maxima of density assigned to deuterium and  
14 the average oxygen site is shorter than a plausible covalent O-D bond length of 0.97 Å as found  
15 in ice VIII(10, 11). This explains that the conventional structure analysis using the single-site  
16 model results in a shorter (average) O-D covalent bond, whereas the deuterium in ice VIII does  
17 not show such spreading distribution (Figure S4).  
18 On the other hand, oxygens show more elongated distributions toward the O-D covalent bond  
19 (Figures 2c and 2d), which corresponds to  $\langle 111 \rangle$  direction in the ice VII structure rather than  
20  $\langle 100 \rangle$  or  $\langle 110 \rangle$  directions. However, the density distributions are not tetrapodal but pyramidal,  
21 meaning that other components such as along  $\langle 100 \rangle$  are not fully excluded. The real disordered  
22 structure would be the combination of dominant displacements toward  $\langle 111 \rangle$  and some other  
23 components with variations. The more diffuse features in the single-crystal data compared to the  
24 powder data would be mainly due to the achieved resolution for the observed diffractions.  
25 Nonetheless, our examinations from two distinct experimental setups, at different neutron  
26 sources, different high-pressure devices, and different detectors, suggest the feature of  $\langle 111 \rangle$   
27 displacement of oxygen is real and intrinsic for ice VII. This is hence consistent with the model  
28 proposed by Nelmes *et al.*(14).  
29 These displacements of oxygen and deuterium were partly proposed in the previous studies(13,  
30 14), but our study shows for the first time unambiguously the three-dimensional distribution in ice  
31 VII by the model-independent MEM approach. Our result shows that the structure of ice VII is  
32 clearly distinct from the single-site model. The ring-like distribution of deuterium can be ascribed  
33 to the time and spatial average of water molecules in different orientations rather than a distortion  
34 of water molecules themselves like DOD bending. Such displacement induces bending of the  
35 hydrogen-bonding networks from an ideal diamond-like network with cubic symmetry.  
36 It should be noted that the density distribution of deuterium also elongates toward oxygens of the  
37 neighboring water molecules. This suggests two possibilities. One explanation is that hydrogen-  
38 bonded water molecules get closer, which means the network structure is modified. The other  
39 explanation is that the interpenetrating hydrogen-bonding network locally displaces along  $\langle 111 \rangle$ .  
40 This would mean that the local structure of ice VII differs from that of ice VIII, the hydrogen-  
41 ordered phase, with displacement along  $\langle 100 \rangle$ .  
42 Relating to the displacement of oxygen along the  $\langle 111 \rangle$  direction, a modulated structure was  
43 previously proposed from single-crystal x-ray diffraction(19, 20). In our single-crystal neutron  
44 diffraction, however, no superlattice reflection was observed similar to any other studies using  
45 powder x-ray and neutron diffraction. There is no technical reason why such reflections cannot be  
46 observed in our experiment because the intensity of the superlattice reflection should be  
47 comparable to that of 111 reflections (see Figure 2 in ref(19)) which were observed in our study.  
48 The origin of the previously reported superlattice reflection remains hence unclear.  
49 In order to reveal the short-range structures of ice VII such as interatomic distances and local  
50 ordering, the correlation functions were derived from the total scattering of powder diffraction  
51 instead of extracted intensities of the Bragg peaks as in the conventional structure refinements  
52 and the MEM analysis. The exact O-H(D) distance in ice  $I_h$  was derived from the total scattering  
53 analysis(21).

1 The total correlation functions  $T(r)$  of ice VII and VIII from powder diffraction at 274 K and 2.2  
2 GPa has a similar profile in the short- $r$  region (Figures 3a and 3b). Assuming that each correlation  
3 has Gaussian type distribution,  $T(r)$  can be divided into several peaks. The representative  
4 geometries are listed in Table 1 with corresponding geometry obtained by the Rietveld analysis  
5 using the single-site model. The Rietveld analysis resulted in the O-D length of 0.9163 (5) Å in ice  
6 VII, significantly shorter than that of 0.9681 (8) Å in ice VIII which agree well with previously  
7 reported values(10, 11). Our fitting of  $T(r)$  gave an O-D distance of 0.9662 (5) Å for ice VII,  
8 proving the suggested similarity of its intramolecular structure with ice VIII(22). The coordination  
9 numbers of the covalent O-D were estimated to be 1.8 for both ices VII and VIII. The slightly small  
10 value from the ideal number 2.0 would be ascribed to the systematic error related to the overall  
11 scaling of the scattering patterns, such as multiple scattering and attenuation. The molecular  
12 geometry of water in ice VII is hence identical to that in ice VIII, *i.e.* the apparently short O-D  
13 length in ice VII results from time- and spatial-average in Rietveld analyses.

14 To compare interatomic correlations at longer distances we discuss the pair distribution function  
15  $G(r)$  instead of  $T(r)$ . Figure 3c shows that both ices VII and VIII have a peak at 0.97 Å, which  
16 corresponds to the O-D covalent bond as discussed for  $T(r)$ . On the other hand, the profiles differ  
17 from each other in the region longer than the lattice parameter  $a_0$  of ice VII. This mean that ice VII  
18 does not have the same interatomic correlation as ice VIII over the distance of the second  
19 nearest neighbors. Especially, ice VIII has a tiny bump at 1.9 Å which corresponds to hydrogen-  
20 bonded O...D whereas that region in ice VII is smooth. Such difference in the correlation function  
21 is attributed to the molecular ordering in each phase. Based on a reported DFT-based  
22 calculation(23), local configurations like ice VIII are not dominant at  $pT$  conditions where ice VII is  
23 stable but other configurations have comparative populations. These are consistent with the  
24 atomic distribution obtained from the MEM analysis in which  $\langle 100 \rangle$  displacements are not  
25 observed.

26

## 27 Discussion

28

29 The atomic distribution observed in the MEM analyses would reflect the dynamic natures of ice  
30 VII. The total scattering analyses revealed that the water molecule has chemically plausible  
31 geometry in ice VII, as expected in the case of ice  $I_h$ (21). The disorder comprises the molecular  
32 orientation and their displacements from the average positions, resulting in the unusual atomic  
33 arrangements of ice VII described by the discrete atomic sites in the single-site and multi-site  
34 models in conventional structure analyses. Spectroscopic studies(24–26) and the quick  
35 transformation from ice VIII to ice VII(2) imply that the disordering of ice VII takes place  
36 dynamically at around 300 K. The atomic distribution is related to such dynamic conversion  
37 among the configurations. The dynamic motions in ice are expressed mainly by two components,  
38 rotation and translation. Their contributions depend on pressure in a contrasting way. At lower  
39 pressures, water molecules have enough space to flip and rotation motion is dominant. Under  
40 higher pressure, the water molecules get closer and become difficult to flip. On the other hand,  
41 reducing the intermolecular distances enhances the probability of translation of deuterium  
42 between neighboring water molecules. The cross-over of two dynamics takes place at around 10  
43 GPa, first suggested from Raman spectroscopy(1) and recently proven from dielectric  
44 measurements(27), and illustrates the origin of previously-reported anomalies: *e.g.* peak widths of  
45 stretching mode(1), phase transition kinetics(2), electrical conductivity(25), and proton  
46 diffusion(26). In conventional structure refinements, ADPs decrease with increasing pressure ( $2 <$   
47  $p < 10$  GPa) and become almost constant above 10 GPa(8, 14, 28). This suggests that atomic  
48 distribution in ice VII will be more localized up to 10 GPa. The localized distribution should be  
49 linked with the suppression of rotational motion.

50 The representation with two types of dynamic movement in ice VII introduces an aspect to  
51 attribute the observed unexpected distribution in ice VII to two features. First, the probability  
52 density is distributed in a ring-like shape around the  $\langle 111 \rangle$  axes. Second, the deuterium also has  
53 elongated distribution toward the oxygen of hydrogen-bonded water. These distributions  
54 correspond to instantaneous deviation from the average position. The ring-like distribution should

1 be related to a precession, assignable to rotational or librational motions of molecules, whereas  
2 the elongation along the hydrogen bond would correspond to the translational motion of  
3 deuterium approaching the hydrogen-bonded neighboring molecule.  
4 In addition to the dynamic nature of ice VII, static configurations also play important roles in the  
5 disordered structure of ice VII. The phase transition boundary between ices VII and VIII are  
6 almost temperature independent below 10 GPa, consistent with an estimation from the Clapeyron  
7 equation ( $dp/dT = \Delta S/\Delta V$ ) with their little volume difference,  $\sim 5 \text{ mm}^3/\text{mol}$  compared to the  
8 Pauling entropy,  $3.37 \text{ J}/(\text{K}\cdot\text{mol})$ . On the other hand, the boundary slope becomes steeper at  
9 higher pressures, suggesting that the volume change between ices VII and VIII is significant in  
10 this pressure regime. *Ab initio* calculation estimated the energy gaps among molecular  
11 configurations to be the smallest at this pressure regime, reproducing the tendency of the order-  
12 disorder phase boundary between ices VII and VIII(23). Our total scattering analysis revealed the  
13 clear difference in intermolecular structures of the disordered phase from the ordered counterpart.  
14 Further investigation at higher pressures can provide direct evidence for the pressure-dependent  
15 variation of the local structure as a result of the probability of dominant configuration. Moreover,  
16 the turning pressure overlaps with where the cross-over of dynamics occurs (27). Fundamental  
17 and detailed diffraction techniques can provide direct and pivotal information on the anomalous  
18 physical properties of ice VII under pressure.  
19 Our findings would also provide an approach to elucidate the behaviors of water molecules during  
20 the phase transition to hydrogen-bond symmetrized ice X. Although spectroscopic studies  
21 showed in the 1990s that ice VII transforms into ice X over 60 GPa in  $\text{H}_2\text{O}$  and 70 GPa in  
22  $\text{D}_2\text{O}$ (29–31), the symmetric structure of ice X has not been confirmed experimentally yet by  
23 neutron diffraction. A powder neutron diffraction study of  $\text{D}_2\text{O}$  up to 60 GPa reported the  
24 elongation of covalently-bonded O-D separation (28). The separation of the deuterium site  
25 between the hydrogen-bonded water molecules also decreases, and its linear extrapolation  
26 proposed an upper limit of the symmetrization to be at 113 GPa. Below 60 GPa, water is  
27 considered to retain its molecular nature from spectroscopic studies(29–31) but the physical  
28 properties of the BCC ice differ from ice VII(32–34), called ice VII'. In this pressure regime, the  
29 bimodal potential curve of deuterium becomes unimodal and quantum tunnelling takes place  
30 dominant. The atomic distribution and the correlation function can provide direct images to  
31 observe the transient states toward the hydrogen bond symmetrization.

## 32 33 34 **Materials and Methods**

### 35 36 **Single-crystal neutron diffraction**

37  
38 The single-crystal diffraction experiment was conducted at the D9 hot neutron single-crystal  
39 diffractometer at the Institut Laue-Langevin (ILL, Grenoble, France). The data of ice VII was  
40 collected at 298 K and 2.2 GPa using a diamond anvil cell specially designed for this study(35).  
41 Single-crystalline specimens of deuterated ice VII were grown directly from a water-alcohol  
42 mixture ( $\text{D}_2\text{O}:\text{MeOD}:\text{EtOD} = 5:4:1$  in volume ratio) by cyclic heating and cooling over 2 GPa. The  
43 pressure was estimated by the ruby fluorescence method(36).

### 44 45 **Powder neutron diffraction**

46 The powder diffraction experiments were conducted at the BL11 (PLANET) beamline(16) of the  
47 Material and Life Science Experimental Facility (MLF) at J-PARC (Ibaraki, Japan) using the MITO  
48 pressure-temperature variable system(37). Powder samples of deuterated ice VII were obtained  
49 by compression of ice at 200 K, below the melting curve of ice phases. The repetitive solid-solid  
50 phase transition contributes to preparing fine powder samples suitable for structure analyses. The  
51 diffraction patterns of ice VII were collected at 2.2 GPa and temperatures of 298 K and 274 K. A  
52 powder diffraction pattern of ice VIII was also collected at 274 K and 2.2 GPa for comparison. The  
53 sample pressures were estimated from the equation of state of ice VII and VIII themselves(8).  
54 The phase transition between ices VII and VIII is a 1<sup>st</sup>-order transition that shows hysteresis so that

1 both phases can metastably exist at approximately 274 K during cooling for ice VII or heating for  
 2 ice VIII before the phase transition occurs.

### 4 MEM analysis

5 The MEM analysis tends to give the most uniform distribution under conditions that satisfy the  
 6 constraints. The information entropy  $S$  and the constraints  $C$  are defined as follows.

$$S = - \sum_r^{\text{unit cell}} \rho(\mathbf{r}) \ln \left( \frac{\rho(\mathbf{r})}{\tau(\mathbf{r}) \sum_r^{\text{unit cell}} \rho(\mathbf{r})} \right), \quad (1)$$

$$C = \frac{1}{N_k} \sum_k \left| \frac{F_o(\mathbf{k}) - F_c(\mathbf{k})}{\sigma F_o(\mathbf{k})} \right|^2 - 1, \quad (2)$$

7 where  $\rho(\mathbf{r})$  is the normalized density of scattering length at  $\mathbf{r}$  in a unit cell and  $\tau(\mathbf{r})$  is the  
 8 normalized density derived from prior information for  $\mathbf{r}$ ,  $N_k$  is the number of structure factors,  $\mathbf{k}$  is  
 9 the reciprocal lattice vector to identify each Bragg reflection,  $F_c$  is the structure factors calculated  
 10 from  $\rho(\mathbf{r})$ . The most probable density distribution which maximizes  $S$  can be derived by a method  
 11 of undetermined Lagrange multipliers ( $\lambda$  and  $\mu$ ).

$$Q = S - \lambda C - \mu \left( \sum_r^{\text{unit cell}} \rho(\mathbf{r}) - 1 \right), \quad (3)$$

12 The third term in Eq. 3 is a constraint for the total normalized scattering length to be one. The  
 13 MEM analyses for both single-crystal and powder diffraction were done using the *Dysnomia*  
 14 program(38) and the practical and detailed schemes are in its manual. The crystal structures and  
 15 density distribution map was drawn with the *VESTA* program(39).

### 16 Total scattering analysis

17 Structure factors,  $S(Q)$ , were derived after intensity corrections for background, absorption, etc.  
 18  $S(Q)$  is related to the atomic pair distribution function  $g(r)$  by Eq. 4. Derived correlation functions  
 19 were analyzed in the forms of the total correlation function (TCF)  $T(r)$  and the pair distribution  
 20 function (PDF)  $G(r)$  defined by Eqs. 5 and 6.

$$Q[S(Q)-1] = \int_0^\infty 4\pi\rho_0 r [g(r)-1] \sin(Qr) dr \quad (4)$$

$$T(r) = 4\pi r \rho_0 g(r) \quad (5)$$

$$G(r) = 4\pi r \rho_0 (g(r) - 1) \quad (6)$$

### 23 Acknowledgments

25 This study was supported by JSPS KAKENHI (grant numbers: 18H05224, 18H01936,  
 26 21K18154), the JSPS-CNRS bilateral joint research grant PRC2191, and the GIMRT program of  
 27 the Institute for Materials Research, Tohoku University (Proposal No. 20K0085).  
 28 Neutron diffraction experiments were performed through the J-PARC user programs (No.  
 29 2020B0139) and the ILL user programs (No. 5-15-624). The experiment at the J-PARC was  
 30 performed using the Lab. III at the Comprehensive Research Organization for Science and  
 31 Society (CROSS) user laboratory. [We acknowledge an important contribution of J. S. Loveday  
 32 which explains and clarifies our findings on the total scattering analysis.](#)

### 35 References

- 36 1. P. Pruzan, J. C. Chervin, M. Gauthier, Raman Spectroscopy Investigation of Ice VII and  
 37 Deuterated Ice VII to 40 GPa. Disorder in Ice VII. *Europhys. Lett.* **13**, 81–87 (1990).
- 38 2. K. Komatsu, *et al.*, Anomalous hydrogen dynamics of the ice VII-VIII transition revealed by  
 39 high-pressure neutron diffraction. *Proc. Natl. Acad. Sci. U. S. A.* **117**, 6356–6361 (2020).



- 1 3. T. Itaka, Simulating proton dynamics in high-pressure ice. *Rev. High Press. Sci. Technol. No Kagaku To Gijutsu* **23**, 124–132 (2013).  
2
- 3 4. M. Benoit, D. Marx, M. Parrinello, Tunnelling and zero-point motion in high-pressure ice.  
4 *Nature* **392**, 258–261 (1998).
- 5 5. M. Benoit, D. Marx, M. Parrinello, Quantum effects on phase transitions in high-pressure  
6 ice. *Comput. Mater. Sci.* **10**, 88–93 (1998).
- 7 6. S. W. Peterson, H. A. Levy, A single-crystal neutron diffraction study of heavy ice. *Acta  
8 Crystallogr.* **10**, 70–76 (1957).
- 9 7. E. Whalley, D. W. Davidson, J. B. R. R. Heath, Dielectric Properties of Ice VII. Ice VIII: A  
10 New Phase of Ice. *J. Chem. Phys.* **45**, 3976–3982 (1966).
- 11 8. S. Klotz, *et al.*, Bulk moduli and equations of state of ice VII and ice VIII. *Phys. Rev. B* **95**,  
12 174111 (2017).
- 13 9. K. Komatsu, *et al.*, Crystal structure of magnesium dichloride decahydrate determined by  
14 X-ray and neutron diffraction under high pressure. *Acta Crystallogr. Sect. B Struct. Sci.  
15 Cryst. Eng. Mater.* **71**, 74–80 (2015).
- 16 10. W. F. Kuhs, J. L. Finney, C. Vettier, D. V. Bliss, Structure and hydrogen ordering in ices  
17 VI, VII, and VIII by neutron powder diffraction. *J. Chem. Phys.* **81**, 3612–3623 (1984).
- 18 11. J. D. Jorgensen, R. A. Beyerlein, N. Watanabe, T. G. Worlton, Structure of D<sub>2</sub>O ice VIII  
19 from in situ powder neutron diffraction. *J. Chem. Phys.* **81**, 3211–3214 (1984).
- 20 12. J.-L. Kuo, M. L. Klein, Structure of Ice-VII and Ice-VIII: A Quantum Mechanical Study. *J.  
21 Phys. Chem. B* **108**, 19634–19639 (2004).
- 22 13. J. D. Jorgensen, T. G. Worlton, Disordered structure of D<sub>2</sub>O ice VII from in situ neutron  
23 powder diffraction. *J. Chem. Phys.* **83**, 329–333 (1985).
- 24 14. R. J. Nelmes, J. S. Loveday, W. G. Marshall, G. Hamel, J. M. Besson, Multisite  
25 Disordered Structure of Ice VII to 20 GPa. *Phys. Rev. Lett.* **81**, 2719–2722 (1998).
- 26 15. C. Knight, S. J. Singer, Site disorder in ice VII arising from hydrogen bond fluctuations. *J.  
27 Phys. Chem. A* **113**, 12433–12438 (2009).
- 28 16. T. Hattori, *et al.*, Design and performance of high-pressure PLANET beamline at pulsed  
29 neutron source at J-PARC. *Nucl. Instruments Methods Phys. Res. Sect. A Accel.  
30 Spectrometers, Detect. Assoc. Equip.* **780**, 55–67 (2015).
- 31 17. J. C. Li, M. Adams, Inelastic incoherent neutron scattering study of the pressure  
32 dependence of ice VII and VIII. *Europhys. Lett.* **34**, 675–680 (1996).
- 33 18. S. Klotz, T. Strässle, C. G. Salzmann, J. Philippe, S. F. Parker, Incoherent inelastic  
34 neutron scattering measurements on ice VII: Are there two kinds of hydrogen bonds in  
35 ice? *Europhys. Lett.* **72**, 576–582 (2005).
- 36 19. P. Loubeyre, R. LeToullec, E. Wolanin, M. Hanfland, D. Husermann, Modulated phases  
37 and proton centring in ice observed by X-ray diffraction up to 170 GPa. *Nature* **397**, 503–  
38 506 (1999).
- 39 20. M. Somayazulu, *et al.*, In situ high-pressure x-ray diffraction study of H<sub>2</sub>O ice VII. *J.*

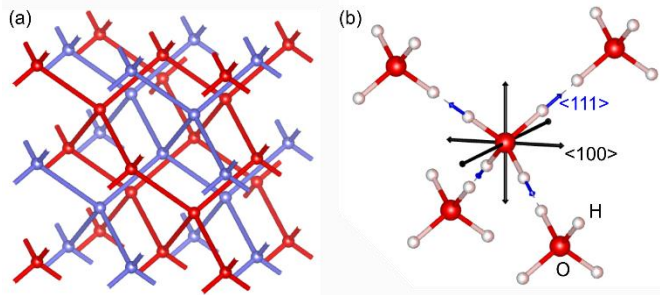
- 1            *Chem. Phys.* **128**, 064510 (2008).
- 2    21.    M. A. Floriano, *et al.*, Direct determination of the intramolecular O-D distance in ice Ih and  
3            Ic by neutron diffraction. *Nature* **329**, 821–823 (1987).
- 4    22.    M. Guthrie, *et al.*, The local structure of ice VII determined by neutron total scattering. *Acta*  
5            *Crystallogr. Sect. A Found. Crystallogr.* **61**, c94–c94 (2005).
- 6    23.    K. Umemoto, R. M. Wentzcovitch, S. de Gironcoli, S. Baroni, Order–disorder phase  
7            boundary between ice VII and VIII obtained by first principles. *Chem. Phys. Lett.* **499**,  
8            236–240 (2010).
- 9    24.    E. Katoh, H. Yamawaki, H. Fujihisa, M. Sakashita, K. Aoki, Protonic diffusion in high-  
10            pressure ice VII. *Science (80-. )*. **295**, 1264–1266 (2002).
- 11   25.    T. Okada, T. Iitaka, T. Yagi, K. Aoki, Electrical conductivity of ice VII. *Sci. Rep.* **4**, 5778  
12            (2014).
- 13   26.    N. Noguchi, T. Okuchi, Self-diffusion of protons in H<sub>2</sub>O ice VII at high pressures: Anomaly  
14            around 10 GPa. *J. Chem. Phys.* **144** (2016).
- 15   27.    R. Yamane, K. Komatsu, H. Kagi, Direct evidence of the proton-dynamics crossover in ice  
16            VII from high-pressure dielectric measurements beyond 10 GPa. *Phys. Rev. B* **104**,  
17            214304 (2021).
- 18   28.    M. Guthrie, *et al.*, Structure and disorder in ice VII on the approach to hydrogen-bond  
19            symmetrization. *Phys. Rev. B* **99**, 184112 (2019).
- 20   29.    K. Aoki, H. Yamawaki, M. Sakashita, H. Fujihisa, Infrared absorption study of the  
21            hydrogen-bond symmetrization in ice to 110 GPa. *Phys. Rev. B* **54**, 15673–15677 (1996).
- 22   30.    A. F. Goncharov, V. V. Struzhkin, M. Somayazulu, R. J. Hemley, H. Mao, Compression of  
23            ice to 210 gigapascals: Infrared evidence for a symmetric hydrogen-bonded phase.  
24            *Science (80-. )*. **273**, 218–220 (1996).
- 25   31.    P. Pruzan, *et al.*, Raman Scattering and X-ray Diffraction of Ice in the Megabar Range.  
26            Occurrence of a Symmetric Disordered Solid above 62 GPa. *J. Phys. Chem. B* **101**,  
27            6230–6233 (2002).
- 28   32.    A. Polian, M. Grimsditch, New high-pressure phase of H<sub>2</sub>O: Ice X. *Phys. Rev. Lett.* **52**,  
29            1312–1314 (1984).
- 30   33.    E. Sugimura, *et al.*, Compression of H<sub>2</sub>O ice to 126 GPa and implications for hydrogen-  
31            bond symmetrization: Synchrotron x-ray diffraction measurements and density-functional  
32            calculations. *Phys. Rev. B* **77**, 214103 (2008).
- 33   34.    A. S. J. Méndez, *et al.*, Bulk modulus of H<sub>2</sub> O across the ice VII-ice X transition measured  
34            by time-resolved x-ray diffraction in dynamic diamond anvil cell experiments. *Phys. Rev. B*  
35            **103**, 1–7 (2021).
- 36   35.    K. Yamashita, *et al.*, A nano-polycrystalline diamond anvil cell with bulk metallic glass  
37            cylinder for single-crystal neutron diffraction. *High Press. Res.* **40**, 88–95 (2020).
- 38   36.    H. Mao, J. Xu, P. M. Bell, Calibration of the ruby pressure gauge to 800 kbar under quasi-  
39            hydrostatic conditions. *J. Geophys. Res.* **91**, 4673 (1986).

- 1 37. K. Komatsu, *et al.*, Development of a new P-T controlling system for neutron-scattering  
2 experiments. *High Press. Res.* **33**, 208–213 (2013).
- 3 38. K. Momma, T. Ikeda, A. A. Belik, F. Izumi, Dysnomia, a computer program for maximum-  
4 entropy method (MEM) analysis and its performance in the MEM-based pattern fitting.  
5 *Powder Diffr.* **28**, 184–193 (2013).
- 6 39. K. Momma, F. Izumi, VESTA 3 for three-dimensional visualization of crystal, volumetric  
7 and morphology data. *J. Appl. Crystallogr.* **44**, 1272–1276 (2011).
- 8  
9

1 **Figures and Tables**

2

3



4

5

6

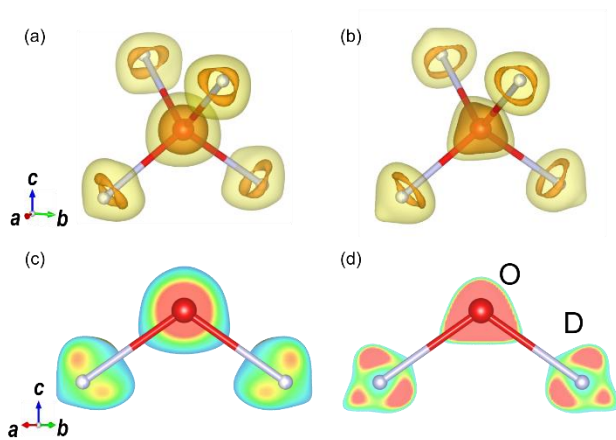
7

8

9

10

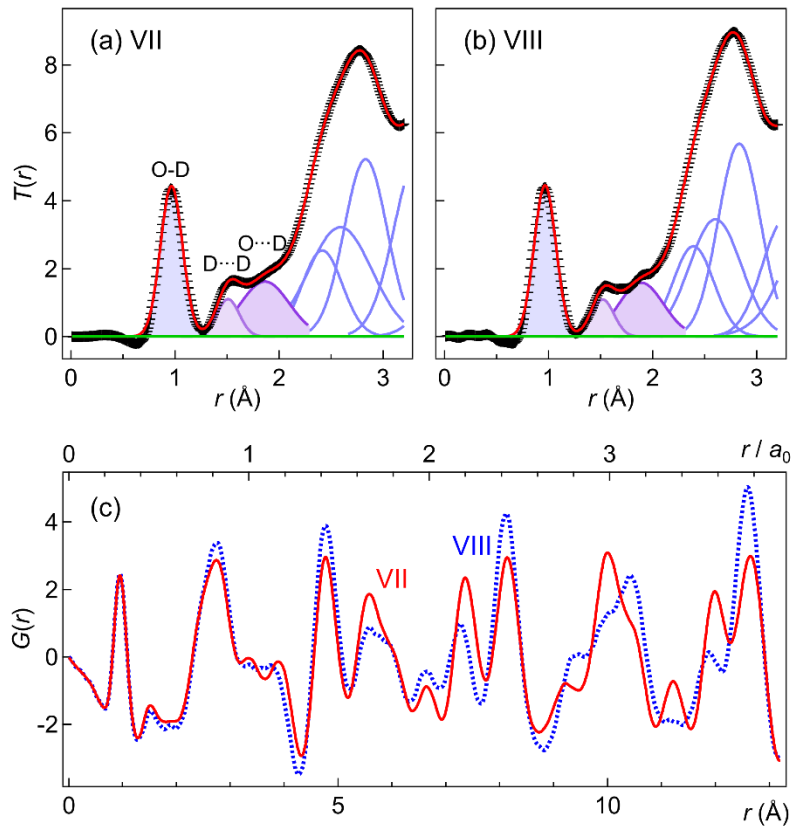
**Figure 1.** Crystal structure of ice VII. (a) Interpenetrating diamond-like hydrogen-bonding networks colored by red and light blue. Balls on the nodes correspond to oxygen while hydrogen is omitted for clarity. (b) Close-up view of water molecules in the same hydrogen-bonding network. Large red and small pink balls correspond to oxygen and hydrogen, respectively.



1  
2  
3  
4  
5  
6  
7  
8

**Figure 2.** Distribution of scattering-length density in ice VII derived from (a) single-crystal data and (b) powder diffraction data both at 298 K and 2.2 GPa. (c) and (d) are cross sections of (a) and (b) on (110) plane, respectively. The oxygens and deuteriums are illustrated as those in the single-site model with O-D = 0.97 Å, as in the water molecule, and  $\angle\text{DOD} = 109.47^\circ$  for comparison. Density decreases from red to blue color.

1



2

3

**Figure 3.** Total correlation functions  $T(r)$  of (a) ice VII and (b) ice VIII at 274 K and 2.2 GPa. Each peak was fitted using Gaussian functions (blue curves). The black cross indicates measured data and the red line corresponds to a profile reproduced from peak fitting. The initial five peaks at  $r < 2.5$  Å are located at the expected positions derived from the Rietveld analysis whereas four peaks up to 4.4 Å were set to be at the maximal positions of the profile. (c) Pair distribution functions  $G(r)$  of ice VII and VIII were obtained at 274 K and 2.2 GPa. Abscissa on top is normalized interatomic distance by lattice parameter  $a_0 = 3.346632$  (13) Å of ice VII determined from the Rietveld analysis.

10

11

1 **Table 1.** Summary of interatomic distances derived from Gaussian peak fitting of correlation  
 2 function  $T(r)$  and Rietveld refinement with reported values.

		VII $_{T(r)}$	VIII $_{T(r)}$	VII $_{Riet}$	VIII $_{Riet}$	VIII	VIII
	unit			This study		ref. 10)	ref. 11)
$r(O-D)$	(Å)	0.9662 (5)*	0.9658 (5)*	0.9163 (5)	0.9681 (8)	0.968 (7)	0.973(11)°
$r(D...D)$	(Å)	1.510 (5)*	1.521 (6)*	1.4963 (10)	1.5498 (14)	1.543 (14)	1.532(12)°
$r(O...D)$	(Å)	1.86 (13)*	1.89 (26)*	1.9820 (5)	1.9304 (8)	1.911 (9)	1.920(10)°
$\angle DOD$	(°)	102.8 (4)*	103.9 (6)*	109.47	106.34 (11)	105.6 (11)	103.8(15)°
$\rho$	(GPa)	2.2	2.2	2.2	2.2	2.4	2.8
$T$	(K)	274	274	274	274	10	269

3

4

5 \* Errors estimated from the SD of peak fitting for  $T(r)$  are given in parenthesis.

6 ° Errors estimated from the refinement procedures are given in parentheses. Riet, Rietveld.

7

8